journal

J. Am. Ceram. Soc., **85** [3] 565–72 (2002)

Sequential Combination of Constituent Oxides in the Synthesis of $Pb(Fe_{1/2}Nb_{1/2})O_3$ by Mechanical Activation

Xingsen Gao, Junmin Xue, and John Wang*,†

Department of Materials Science, National University of Singapore, Singapore 119260

Ting Yu and Ze Xiang Shen

Department of Physics, National University of Singapore, Singapore 119260

$Pb(Fe_{1/2}Nb_{1/2})O_3$ (PFN) has been successfully synthesized via a novel mechanical activation of mixed oxides and columbite precursor consisting of lead oxide and $FeNbO_4$. A nanocrystalline perovskite phase 5–15 nm in crystallite size was formed after 30 h of mechanical activation at room temperature for both types of starting materials. However, the nanocrystalline PFN phase derived from the mixed oxides of PbO, Fe_2O_3, and Nb_2O_5 is unstable, and develops pyrochlore phases when calcined at 500°–900°C, while no pyrochlore phase is observed for the material derived from the columbite precursor consisting of PbO and $FeNbO_5$. Different sintering behavior and dielectric properties were also observed between the two types of PFN. These differences are accounted for by the compositional inhomogeneity in the material derived from the mixed oxides, as was revealed by Raman spectroscopic studies. This suggests that mechanical activation is analogous to thermal activation, where the phase development is strongly dependent on the sequence of combining the constituent oxides.

I. Introduction

LEAD IRON NIOBIUM OXIDE ($Pb(Fe_{1/2}Nb_{1/2})O_3$) (PFN) is one of the important candidate materials for multilayer capacitors and other electronic devices because of its excellent dielectric properties and low firing temperature.[1,2] Moreover, it undergoes a diffuse ferroelectric phase transition at ~380 K and an antiferromagnetic phase transition at ~145 K,[3,4] thus making it a ferroelectromagnetic material.[4] Studies on the coupling of the electrical and magnetic ordering of PFN could lead to insights into the mechanism of ferroelectricity and magnetism in this complex perovskite structure, which may be used for many applications in new electronic devices.

Considerable efforts have been made to enhance the dielectric properties of PFN. Several processing techniques, including solid-state reaction,[5] the columbite method,[6] sol–gel,[7] molten salt,[8] and the coprecipitation method,[9,10] have been attempted to refine the required microstrucure. However, a relatively high sintering temperature is needed for obtaining a high density and desirable dielectric properties for the materials derived from most of these processing techniques.

Mechanical activation is a novel synthesis technique for nanocrystalline materials. Following the pioneering work of Benjamin,[11] mechanical alloying was extended to several nanocrystalline materials.[12,13] Recently, mechanical activation has been successfully devised for the preparation of lead-based relaxor ferroelectrics, such as $Pb(Mg_{1/3}Nb_{2/3})O_3$,[14] $Pb(Zn_{1/3}Nb_{2/3})O_3$ (PZN),[15] and $Pb(Fe_{2/3}W_{1/3})O_3$ (PFW).[16] Compared to conventional ceramic processing, it can dramatically refine the particle and crystallite sizes, enhancing the activity of solid phases and lowering the sintering temperature of ceramic materials. Moreover, the pyrochlore phases, which exhibit a low dielectric constant and always occur as intermediate phases in the conventional solid-state reaction of relaxor ferroelectrics,[5] can be bypassed by mechanical activation, hence, dramatically improving the dielectric properties.[14,15]

A considerable difference has been observed between mechanical activation and thermal activation in triggering a new ceramic phase.[14–16] However, few investigations have been made into the effects of the sequence of combining constituent oxides in mechanical activation, although a dramatic effect on the phase formation and the resulting characteristics of the nanocrystalline phase have been observed in the case of thermal activation.[16] To the best of the authors' knowledge, there is no report on the synthesis of PFN by mechanical activation. In this paper, we investigate the formation of PFN via mechanical activation from two different types of starting materials, mixed oxides and a columbite precursor consisting of $FeNbO_4$ and PbO, to understand the effects of the sequence of combining the oxides in mechanical activation on the phase formation and characteristics of nanocrystalline PFN. Its effects on the phase stability, sintering behavior, and the resulting dielectric properties are also of interest.

II. Experimental Procedure

The starting materials used in this work are commercially available PbO (99% purity, J. T. Baker, Inc., Phillipsburg, NJ), Fe_2O_3 (99% purity, J. T. Baker, Inc.), and Nb_2O_5 (99% purity, Sigma–Aldrich Corp., St. Louis, MO). To prepare the mixed oxides, appropriate amounts of PbO, Fe_2O_3, and Nb_2O_5 were mixed according to the stoichiometric composition of $Pb(Fe_{1/2}Nb_{1/2})O_3$ by ball-milling in ethanol using zirconia balls as the media for 12 h. The resulting oxide mixture was sieved and consequently loaded in a cylindrical vial of stainless steel 40 mm in diameter and 40 mm in length, with one stainless steel ball 12.7 mm in diameter inside. Mechanical activation was conducted for various time periods in the range of 0–30 h using a shaker mill operated at ~900 rpm. To prepare the columbite precursor, Nb_2O_5 and Fe_2O_3 were mixed and then calcined at 1000°C for 4 h. Mechanical activation of PbO with $FeNbO_4$ was conducted in the same manner as the mixed oxides. The ceramic compositions derived from the two types of starting materials were pelleted and then sintered at temperatures ranging from 900°–1200°C for 2 h at a heating rate of 2°C/min, followed by phase identification using X-ray diffractometry (XRD). For dielectric measurement, silver paste was applied on both sides of the pellets and fired at 600°C for 30 min.

S. Trolier-McKinstry—contributing editor

Manuscript No. 187849. Received May 4, 2001; approved October 18, 2001.

This work was supported by the National University of Singapore and Institute of Materials Research and Engineering (IMRE).

*Member, American Ceramic Society.

†Author to whom correspondence should be addressed.

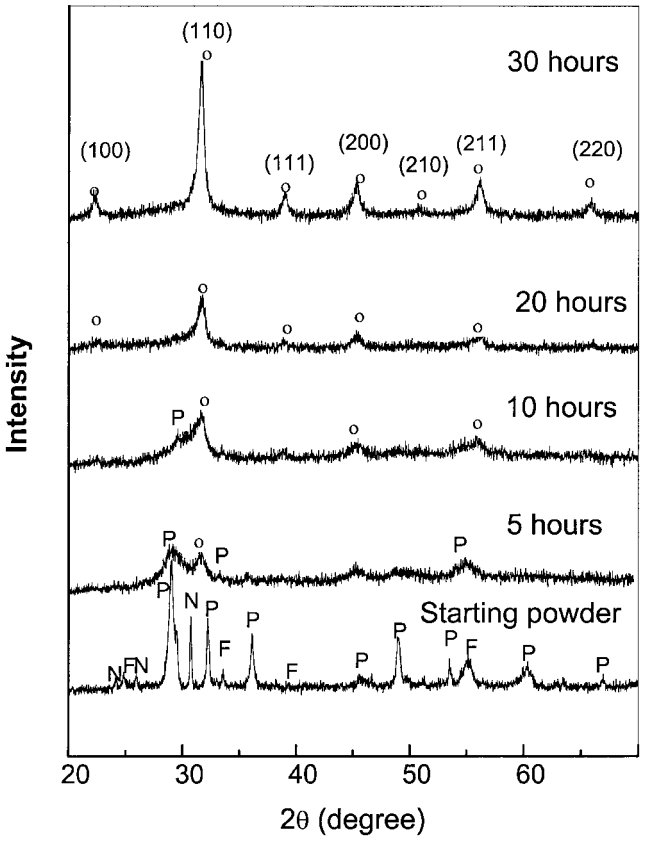

Fig. 1. XRD patterns of the oxide mixture of PbO, Fe_2O_3, and Nb_2O_5 subjected to various periods of mechanical activation from 0 to 30 h ("o": perovskite of PFN; "P": PbO; "N": Nb_2O_5; "F": Fe_2O_3).

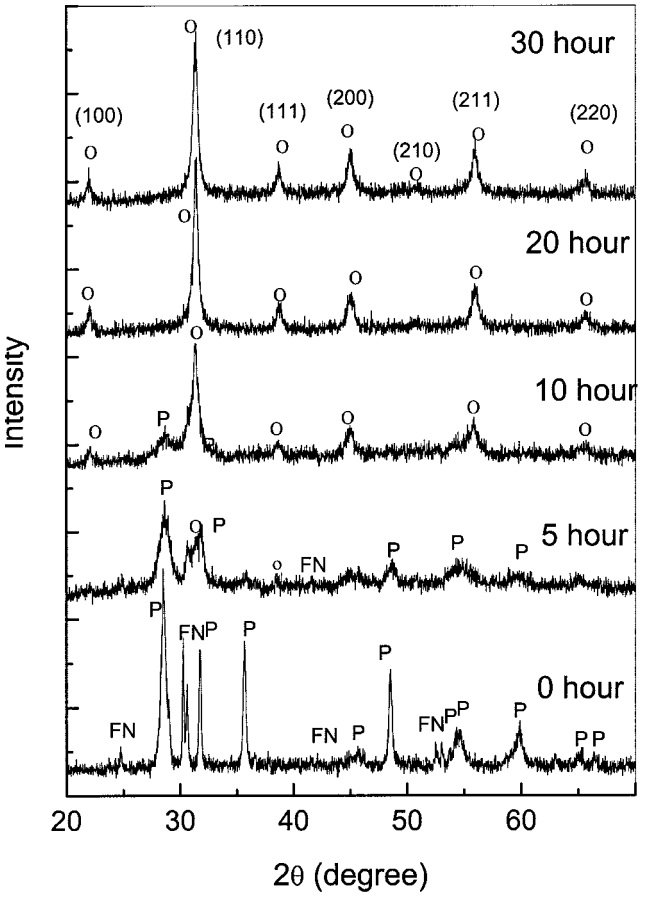

Fig. 3. XRD patterns of the columbite precursor of PbO and $FeNbO_4$ when subjected to various periods of mechanical activation from 0 to 30 h ("o": perovskite PFN; "P": PbO; "FN": $FeNbO_4$).

The powders derived from mechanical activation were also examined using XRD (Cu*K*α radiation, Model X'pert, Philips, Eindhoven, The Netherlands). Their thermal behaviors were characterized using differential thermal analysis (DTA; DuPont, Wilmington, DE) and differential scanning calorimetry (DSC; DuPont). A transmission electron microscope (TEM; Model 100 CX, JEOL, Tokyo, Japan) was used to study their particle and crystallite characteristics. A scanning electron microscope (SEM; Model XL 30, Philips) was also used to determine the particle characteristics as well as the microstructures of sintered ceramic bodies. Micro-Raman spectra were measured at room temperature in the backscattering geometry using a single-grating Raman spectrometer (Model Spex 1702/04, Jobin Yvon, France). The sintered density was measured using the Archimedes method in deionized water. An LCR meter (Model HP 4284A, Hewlett–Packard, Tokyo, Japan) was used to measure the dielectric properties of the sintered PFN over the temperature range of 20°–160°C. A high resistance meter (Model HP 4339B, Hewlett–Packard) and an impedance gain/phase analyzer (Model SI 11260, Solatron, Bloomington, CA) were used to measure the dc conductivity and impedance spectrum, respectively.

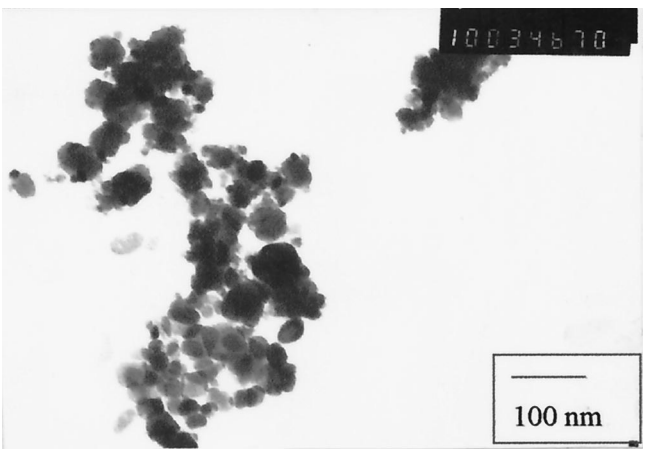

Fig. 2. TEM micrograph showing nanosized particles of the PFN derived from PbO, Fe_2O_3, and Nb_2O_5 subjected to 30 h of mechanical activation.

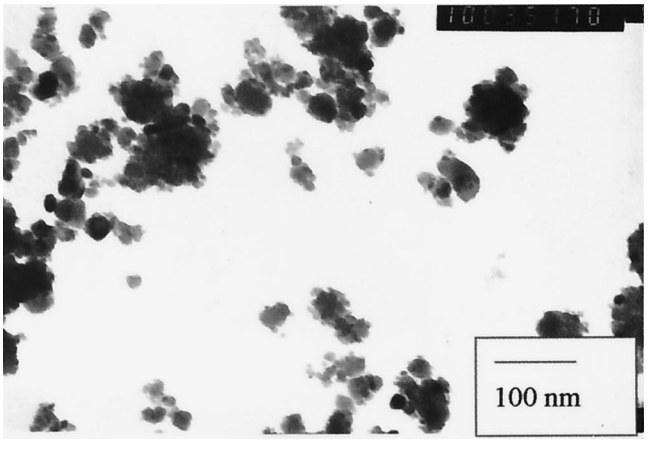

Fig. 4. TEM micrograph showing the nanosized particles of PFN derived from the columbite precursor of PbO and $FeNbO_4$ subjected to 30 h of mechanical activation.

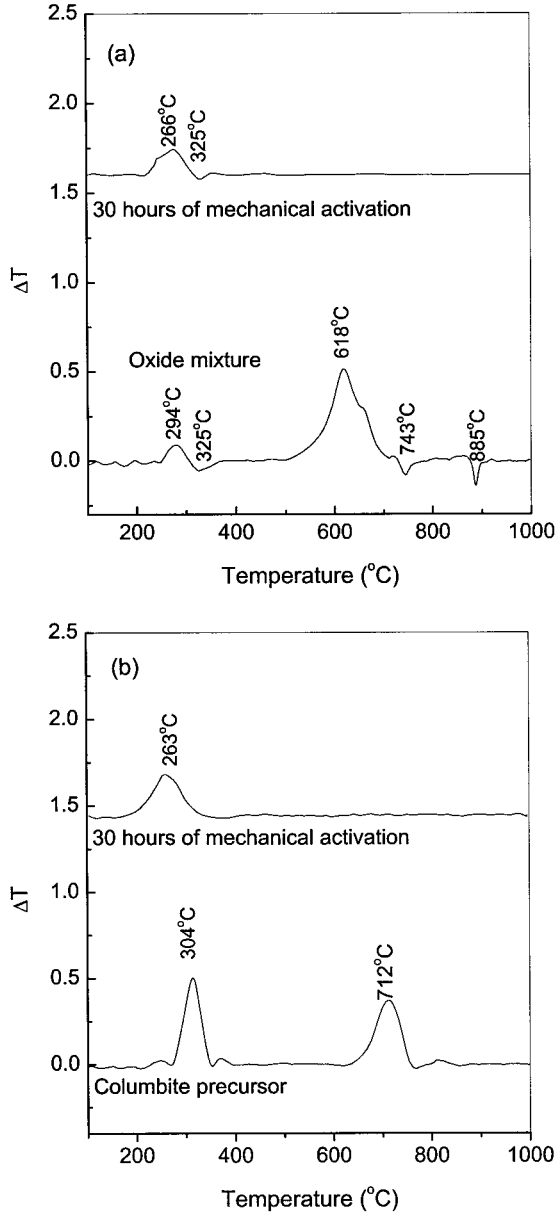

Fig. 5. DTA traces of the PFN derived from mixed oxides and columbite precursor, respectively, along with those of unactivated oxide compositions: (a) mixed oxides of PbO, Fe_2O_3, and Nb_2O_5 and (b) columbite precursor of PbO and $FeNbO_4$.

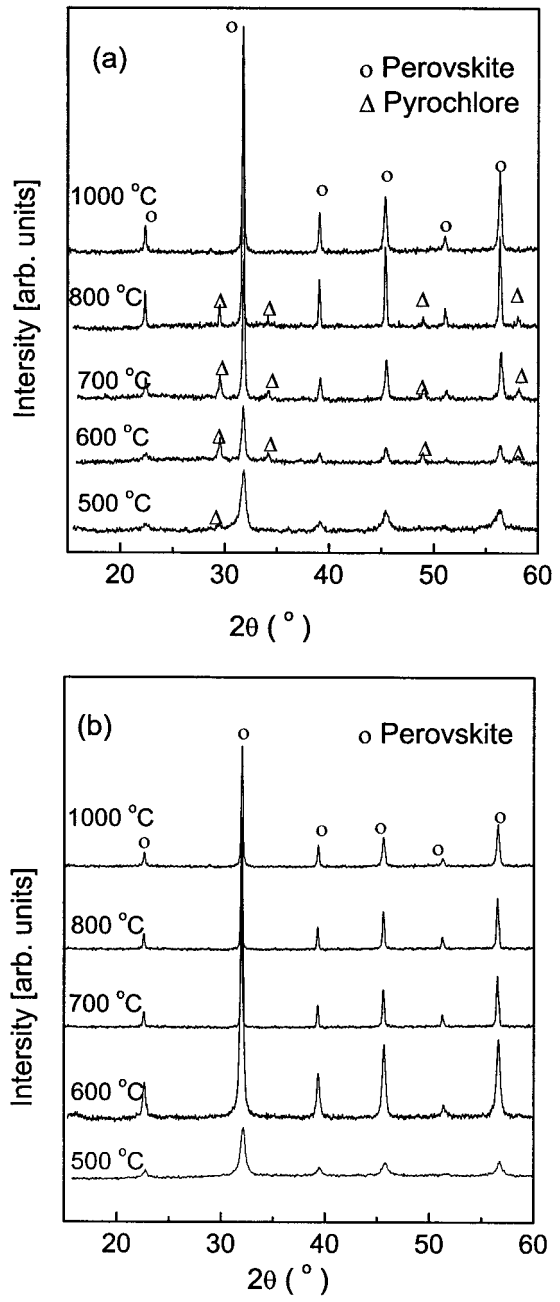

Fig. 6. XRD traces of the compositions calcined at varying temperatures showing the thermal stability of: (a) PFN derived from mixed oxides of PbO, Fe_2O_3, and Nb_2O_5 subjected to 30 h of mechanical activation and (b) PFN derived from PbO and $FeNbO_4$ subjected to 30 h of mechanical activation.

III. Results and Discussion

Figure 1 shows the XRD patterns of the mixed oxides of PbO, Fe_2O_3, and Nb_2O_5 subjected to mechanical activation for various time periods. The starting oxide mixture exhibits the peaks of lead oxide, iron oxide, and niobium oxide. After 5 h of mechanical activation, a perovskite PFN phase occurs, as is indicated by the broad peak centered at 2θ of ~32°, although PbO (111) is still the principal phase that has undergone a degree of amorphization. Further mechanical activation enhances the amount of perovskite phase formed at the expense of lead oxide. After 20 h of mechanical activation, a well-established perovskite phase was evident, although a trace amount of residual lead oxide still existed, as is indicated by the small hump centered at 2θ of 29.0°. Extending the mechanical activation to 30 h sharpens the XRD peaks, indicating an increasing crystallinity of PFN with the extension of mechanical activation time. The average crystallite size at 30 h of mechanical activation was calculated to be ~12 nm using Scherrer's equation, based on the half-width of the PFN (110) peak.[17] As can be seen from the TEM micrograph in Fig. 2, the activation-derived PFN powders consist of nanosized particles ~15–35 nm in size, although they occur as particle agglomerates, which can be observed in the TEM and SEM micrographs.

The X-ray spectra of the powders derived from the columbite precursor after mechanical activation for various durations are shown in Fig. 3. As expected, the unactivated precursor exhibits peaks of lead oxide and $FeNbO_4$ phase. After 5 h of mechanical activation, a notable amount of perovskite phase is observed, along with the broad peaks of PbO and columbite phase. The nanocrystalline PFN phase is well-established after 20 h of mechanical activation. Further extending of mechanical activation to 30 h resulted in an improvement of the crystallinity of the perovskite phase, as is indicated by the sharpened diffraction peak at 2θ of ~32°. Similar to the PFN composition derived from the mechanical activation of mixed oxides, there was a trace amount of

residual lead oxide after 30 h of mechanical activation, as is indicated by the small hump centered at 2θ of 29.0°. The particle size and morphology of the PFN phase derived from the mechanical activation of PbO and $FeNbO_4$ are illustrated by the TEM micrograph in Fig. 4. It consists of nanosized particles ~20–35 nm in size with a degree of particle agglomeration, which is similar to that derived from the mixed oxides. The average crystallite size is ~12 nm, using Scherer's equation.[17]

The phase stability of the two powders mentioned above was examined using DTA, the results of which are shown in Figs. 5(a) and (b). In Fig. 5(a), two strong exotherms and three main endotherms are observed for the unactivated mixed oxides. The exotherm at ~294°C is related to the phase transition of lead oxide with increasing temperature, and the one at ~618°C is attributed to the formation of the pyrochlore phase. The endotherm at ~743° is caused by the conversion of one pyrochlore phase into another, and the endotherm at 885°C is related to the formation of perovskite PFN. These thermal events are in agreement with those in a previous study,[18] and were also confirmed by the phase analyses using XRD in this work. Moreover, there is a small endotherm at ~325°C, which can be accounted for by the burn-off of residual ethanol derived from the milling solvent.[19] After 30 h of mechanical activation, the endotherms and exotherms related to the phase transition of lead oxide and the formation of pyrochlore phases and a perovskite phase have disappeared, indicating the formation of PFN, triggered by mechanical activation, as is shown by XRD phase analysis. Only one minor endotherm, caused by the burn-off of ethanol residuals at ~325°C, and a broad exotherm at ~266°C, were observed. The broad exotherm was caused by the phase transition of residual PbO from the Massicot to the Litharge phase.[20] Compared to that in the unactivated composition, the transition temperature was broadened and lowered slightly, as the mechanical activation had significantly refined the crystallite size and created defects in the PbO.[21] As is shown in Fig. 5(b), a DTA trace of the unactivated mixture of PbO and $FeNbO_4$ exhibits two exotherms, the first one, at ~304°C, relating to the phase transition of lead oxide, and the second one, at ~712°C, relating to the formation of a perovskite phase, which agrees with a previous report.[6] As was confirmed by phase analysis using XRD in this work, the pyrochlore phase evolved little as a transitional phase before the formation of the perovskite phase with increasing temperature. After 30 h of mechanical activation, the broad exotherm, at ~260°C, caused by the phase transition of residual lead oxide, was the only one left, indicating that the formation of the perovskite phase was largely completed by mechanical activation, as was shown by the results of XRD phase analysis in Fig. 3.

Figure 6(a) shows the XRD patterns of the compositions derived from the mechanical activation of mixed oxides after calcination at various temperatures. The pyrochlore phase was observed at temperatures above 500°C, and it peaked at ~600°C. A higher calcination temperature steadily eliminates the pyrochlore phase. In comparison, the nanocrystallite PFN phase derived from columbite precursor remains the only crystalline phase over the entire calcination temperature range of 400° to 900°C, as is shown in Fig. 6(b).

To understand the difference between the thermal stabilities of the two PFN phases derived from mixed oxides and columbite precursors, Raman spectroscopic studies were conducted. For comparison purposes, a single-phase perovskite PFN prepared by solid-state reaction was also characterized using the Raman spectrometer. As is shown in Fig. 7, the α-Fe_2O_3 phase was observed with the perovskite PFN phase in the material derived from the mixed oxides,[22] although Nb_2O_5 was not detected. In contrast, only the PFN phase was observed for the material derived from the columbite precursor. It is obvious that Fe_2O_3 was left out in the former, although this was not revealed by phase analysis using XRD. Upon calcination with increasing temperature, the compositional inhomogeneity, in association with residual oxides, led to the formation of the pyrochlore phase.

Mechanical activation has been observed to be fundamentally different from thermal activation in several aspects. For example, it skips the transitional pyrochlores, indicating that the phase

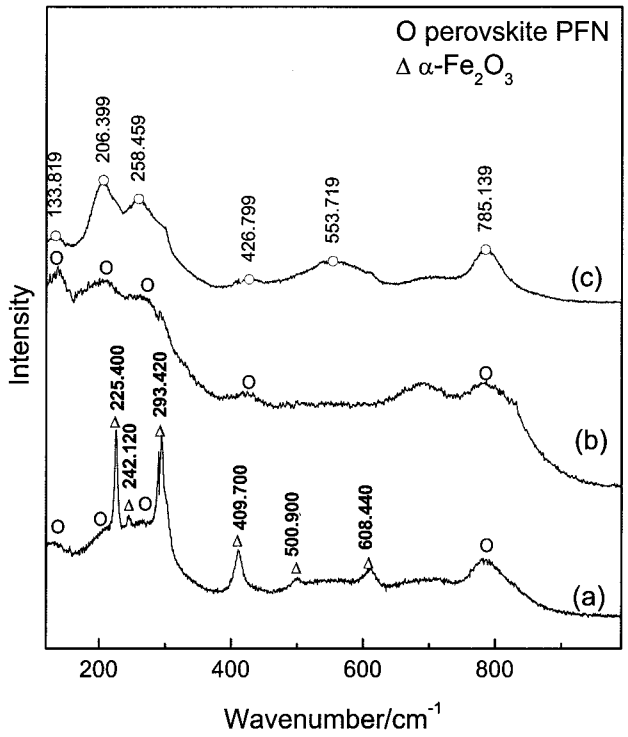

Fig. 7. Raman spectrum of the PFN: (a) derived from mechanical activation of mixed oxides of PbO, Fe_2O_3, and Nb_2O_5; (b) derived from mechanical activation of columbite precursor of PbO and $FeNbO_4$; and (c) perovskite PFN phase prepared by solid-state reaction.

formation occurs via a completely different mechanism. It has been proposed that the formation of the nanocrystalline perovskite phase, triggered by mechanical activation, is not a consequence of traditional interfacial reactions and diffusions.[23] The observed inhomogeneity in phase distribution of the material derived from mixed oxides can be accounted for by the lower reactivity of Fe_2O_3, in comparison to those of PbO and Nb_2O_5, although the growth of PFN nanocrystallites triggered by mechanical processes may not be a result of long distance diffusion, as was proposed by Bellon and Averback.[24] Fe_2O_3 is much more inert than either PbO or Nb_2O_5. For example, the thermal diffusion rate of Fe^{3+}

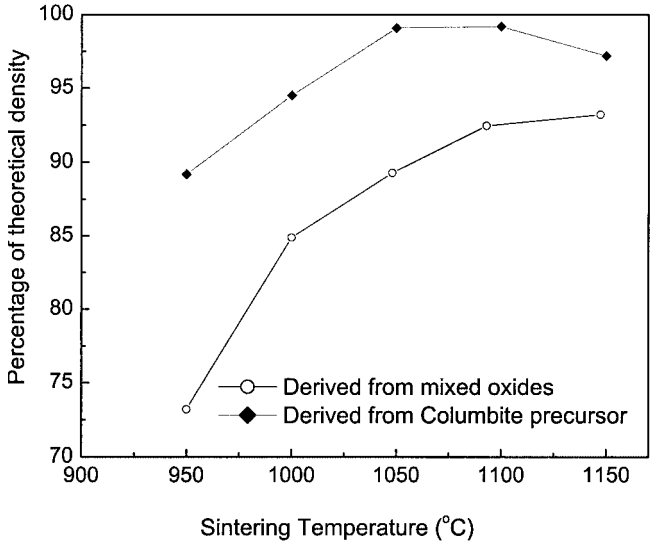

Fig. 8. Sintered density as a function of sintering temperature for PFN derived from mixed oxides and columbite precursor, respectively.

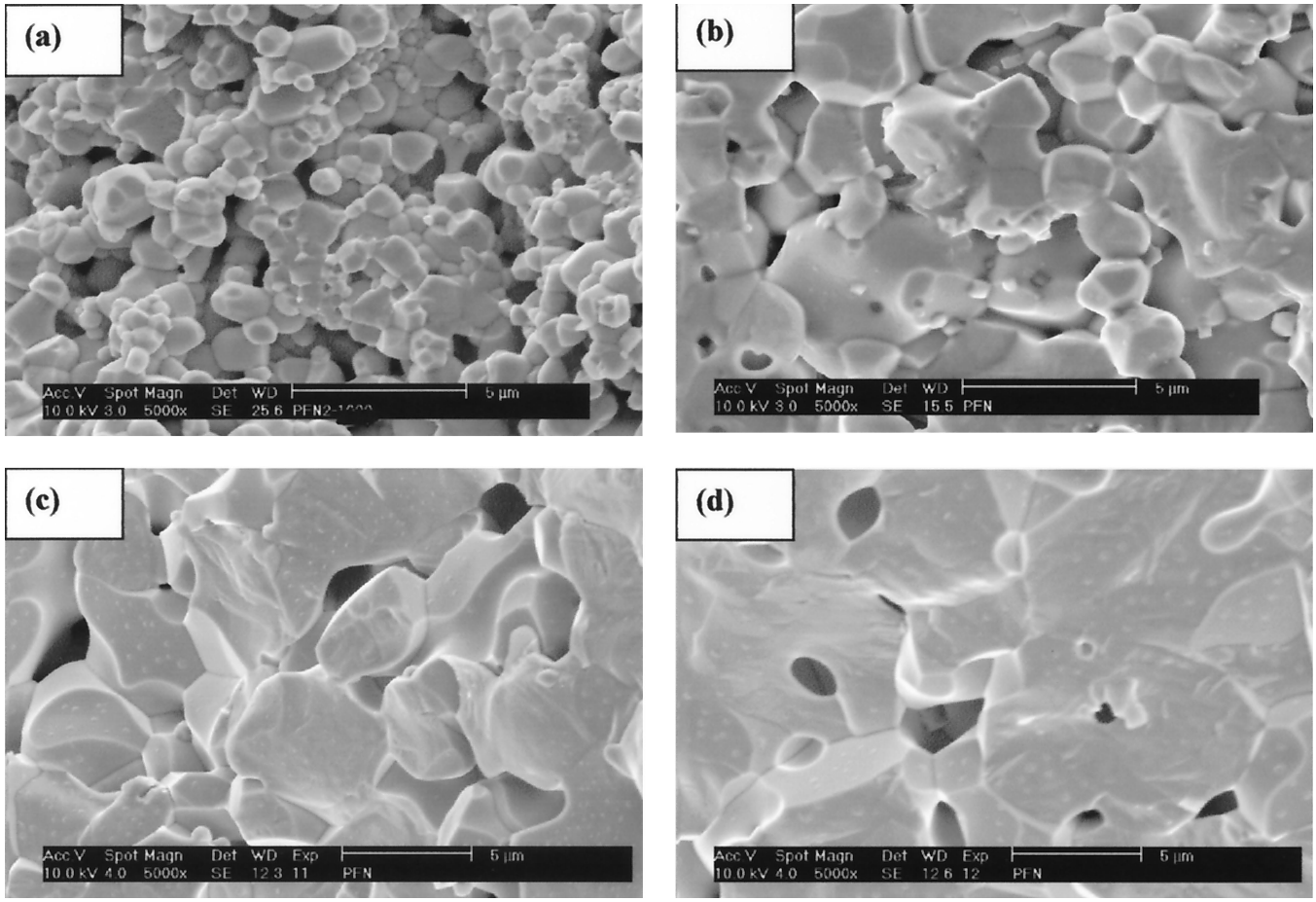

Fig. 9. Fracture surfaces of PFN derived from mechanical activation of mixed oxides of PbO, Fe_2O_3, and Nb_2O_5 sintered at (a) 950°, (b) 1000°, (c) 1100°, and (d) 1150°C.

(activation energy in Fe_2O_3 of 469 kJ/mol and a frequency factor D_0 of 1.3×106 cm^2/s at 760°–1300°C)[25] is much lower than that of Nb^{5+} (activation energy in Nb_2O_5 of 118.1 kJ/mol and a frequency factor of 0.38 cm^2/s at 500°–900°C).[25] Therefore, certain Fe_2O_3 was not combined into the perovskite structure by mechanical activation. Residual Fe_2O_3 remains as fine crystallites, as has been detected by Raman spectroscopy.

The sintering behaviors of the PFN derived from the mixed oxides and columbite precursor are illustrated in Fig. 8. The material derived from mixed oxides shows an increase in sintered density over the temperature range of 950°–1150°C. However, the maximum sintered density is limited to <93% theoretical density (TD). In contrast, the PFN derived from the columbite precursor shows an increase in sintered density to 99% TD at 1050°C. A further increase in the sintering temperature led to a slight drop in density at 1150°C. Therefore, its sintered density is much higher at each sintering temperature than that of the PFN derived from the mixed oxides.

Figures 9(a)–(d) show the fracture surfaces of PFN sintered at the temperatures ranging from 950°–1150°C, derived from mechanical activation of mixed oxides of PbO, Fe_2O_3, and Nb_2O_5. At 950°C, a very porous surface with an average grain size of ~1.5 μm was observed. With an increase in the sintering temperature, the average grain size increases steadily to ~4 μm at 1000°C and ~7 μm at 1100°C. At the same time, the fracture surface becomes less porous. However, there exists a network of intergranular pores of ~2 μm in size, even when sintered at 1150°C. The fracture surfaces of the PFN derived from mechanical activation of columbite precursor are shown in Figs. 10(a)–(d). Compared to those in Figs. 9(a)–(d), they exhibit a much denser fracture surface at each sintering temperature, with few pores occurring at the intergranuar positions. The grain size is also smaller than that of the material derived from mixed oxides at each sintering temperature. It increases gradually from ~0.8 μm at 1000°C to ~4 μm at 1100°C. At 1150°C, coarsened grains and intergranular pores were observed, which can be ascribed to the over-sintering, such that loss of lead and grain coarsening occur at a high temperature. The above difference in sintering behaviors and microstructure between the PFNs derived from mixed oxides and columbite precursor, respectively, can be accounted for by their difference in particle and crystallite characteristics in the as-synthesized state from mechanical activation. As was discussed earlier, a pyrochlore phase was involved as a transitional phase with increasing temperature for the material derived from mixed oxides. Because the molar volume of the pyrochlore phase is larger than that of the perovskite phase, the conversion from the pyrochlore phase to the perovskite phase can create pores. At the same time, the composition heterogeneity can also result in Kirkendall swelling[26–28] because of the different diffusion rates of the remaining phases. In comparison, no pyrochlore phase was involved in the PFN derived from the columbite precursor, and the composition is also homogeneous, leading to a higher sintering density.

The dielectric constant and dielectric loss of PFN derived from the two types of starting materials at various sintering temperatures are summarized in Table I. For the ceramic derived from mixed oxides and sintered at 950°C, a peak dielectric constant of ~5000 was measured at 1 kHz. The dielectric constant increases dramatically with a sintering temperature above 1000°C, e.g., a dielectric constant of 11 700 at 1000°C and 17 500 at 1050°C can be observed. At sintering temperatures of >1100°C, the material became very conductive, leading to an unrealistically high dielectric constant and extremely large dielectric loss. In comparison, a more realistic dielectric constant and a lower value of dielectric loss were

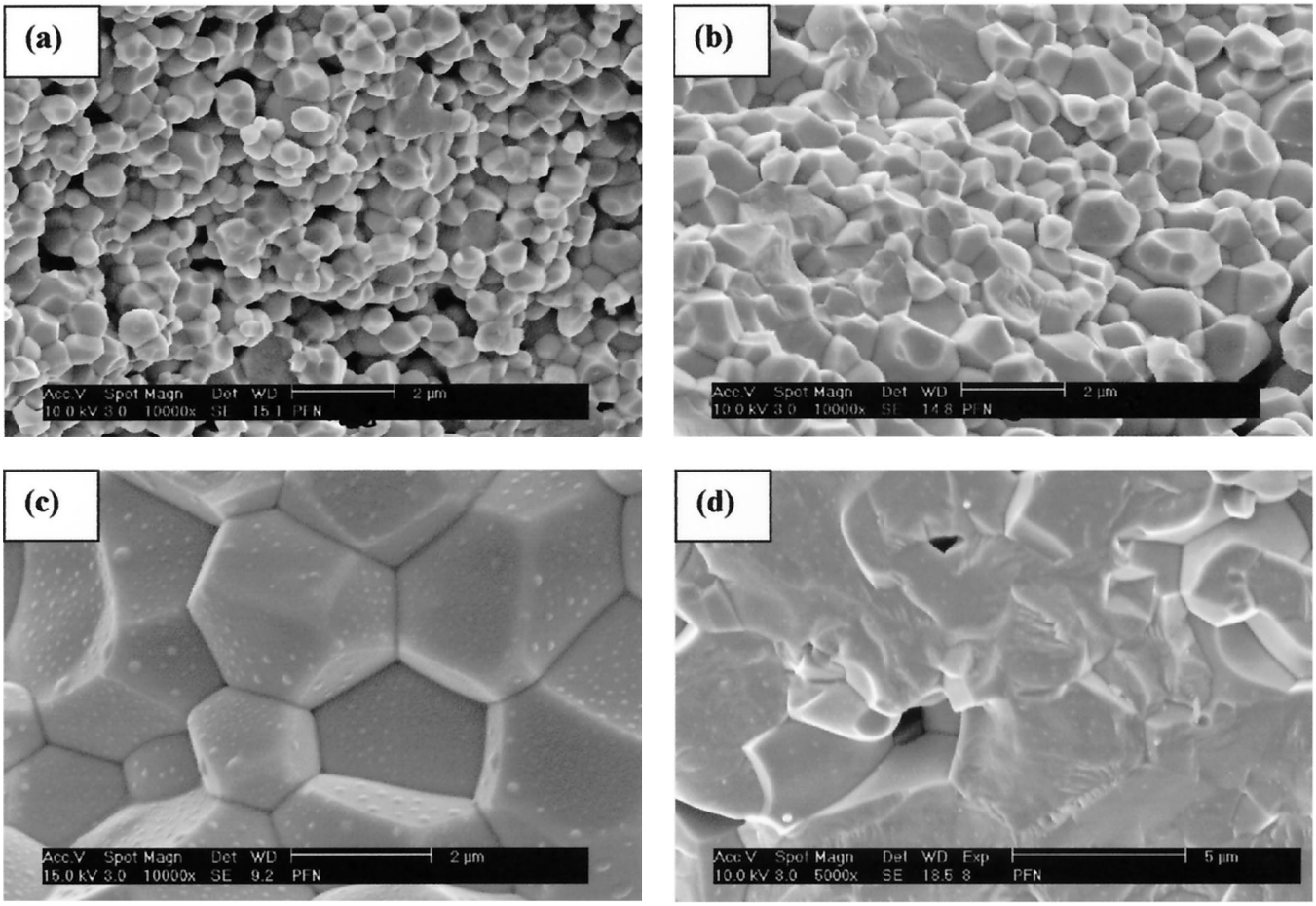

Fig. 10. Fracture surfaces of PFN derived from the columbite precursor of PbO and $FeNbO_4$ sintered at (a) 950°, (b) 1000°, (c) 1100°, and (d) 1150°C.

observed for the PFN derived from the columbite precursor, although they also increase steadily as the sintering temperature increases. A peak dielectric constant of ~17 000 and dielectric loss of ~0.36, and a dielectric constant of ~27 000 and dielectric loss of ~0.45, were measured for the ceramic sintered at 1000° and 1100°C, respectively. These dielectric constants and dielectric losses are comparable to those of the materials derived from other processing routes. For example, a dielectric constant of ~20 000 and a dielectric loss of ~0.2 at the sintering temperature 1075°C, and a dielectric constant of 100 000 and dielectric loss of ~6 at the sintering temperature of 1175°C, were reported[29]).

The high dielectric constant and dielectric loss listed above can be ascribed to the trapped charge carriers, the hopping of which can result in an extra dielectric response in addition to the dipole response. A relatively high conductivity can also result in an extremely high dielectric loss, as was discussed by Jonscher.[30] The high conductivity and hopping of charge carriers in association with Fe^{2+}/Fe^{3+} in PFN was shown in the Mössbauer study[31,32] in the PFN and impedance analysis of PFW–PFN–PZN. In this work, iron contamination from the stainless steel ball and activation vial was calculated to be equivalent to 0.2% iron oxide. For example, the following equilibrium can occur, generating further conductivity from the oxygen vacancies:

$$O_O \rightleftarrows V_O^{\cdot\cdot} + 2Fe'_{Fe} + \frac{1}{2}O_2(g)$$

The occurrence of charge carriers is strongly affected by the compositional homogeneity of PFN and sintering temperature. In the nanocrystalline PFN derived from the mechanical activation of columbite precursor, little residual Fe_2O_3 was detected, and no transitional pyrochlore phase developed with an increase in temperature. Therefore, Fe^{3+} are largely locked in the B-sites of the perovskite structure, making the hopping process difficult, although the iron contamination can result in the formation of Fe^{2+} at the sintering temperature. In contrast, there is a considerable degree of compositional inhomogeneity in the PFN derived from the mechanical activation of mixed oxides, as was confirmed by the experimental results of Raman spectrometry. Any residual Fe_2O_3 with iron contamination in sintered PFN will create an opportunity for the Fe^{3+}/Fe^{2+} hopping to take place and, therefore, lead to a high conductivity. As a result, the resistivity from the dc measurement of the former is much higher than that of the latter (3.4×10^7 Ω·cm for the PFN derived from the columbite precursor and 1.9×10^6 Ω·cm for the PFN derived from the mixed oxides).

Table I. Maximum Dielectric Constant and Corresponding Dielectric Loss at 1 kHz for PFN Derived from Mixed Oxides and Columbite Precursor at Various Sintering Temperatures

	Mixed oxides		Columbite precursor	
Sintering temperature (°C)	Dielectric constant	Dielectric loss	Dielectric constant	Dielectric loss
950	5005	0.455	5008	0.462
1000	14499	0.257	17284	0.362
1050	15520	0.584	19377	0.482
1100	86489	5.674	27028	0.452
1150	98464	7.274	36548	0.597

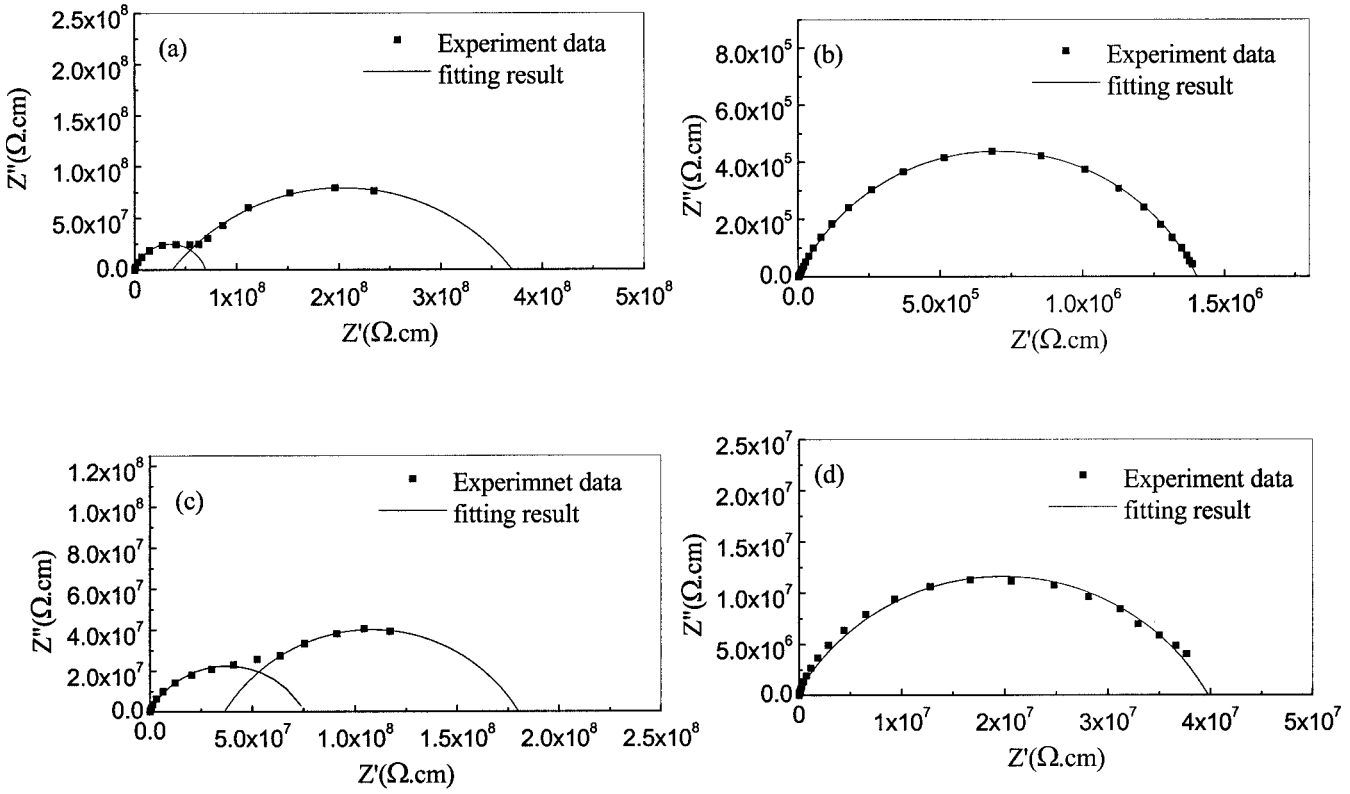

Fig. 11. Cole–Cole impedance plots for the PFNs (a) sintered at 1000°C derived from mechanical activation of mixed oxides, (b) sintered at 1100°C derived from mechanical activation of mixed oxides, (c) sintered at 1000°C derived from mechanical activation of the columbite precursor, respectively, and (d) sintered at 1100°C derived from mechanical activation of the columbite precursor, respectively

The impedance plots for PFN derived from both types of starting materials are shown in Fig. 11. Two depressed semicircles were observed in the PFN derived from mixed oxides sintered at 950°C. The smaller one can be ascribed to the bulk effect, corresponding to the bulk resistance $\sim 7.0 \times 10^7$ Ω·cm. The bigger one is caused by the grain boundary effect, the resistance of which is $\sim 3.7 \times 10^8$ Ω·cm and is much higher than that of the bulk effect. When sintered at 1100°C, only one depressed semicircle at $\sim 1.4 \times 10^6$ Ω·cm was observed. For the PFN derived from the columbite precursor and sintered at 950°C, the impedance plot also shows two semicircles, corresponding to the bulk resistance of 7.3×10^7 Ω·cm and grain boundary resistance of 1.8×10^8 Ω·cm, respectively. For the PFN derived from the columbite precursor and sintered at 1100°C, the bulk resistance is $\sim 4.0 \times 10^7$ Ω·cm and the grain-boundary effect has disappeared. These experimental results show that there is an increase in conductivity with an increasing sintering temperature for both types of PFN, in association with a decrease in resistance from both bulk and grain boundary. This is expected based on microstructure

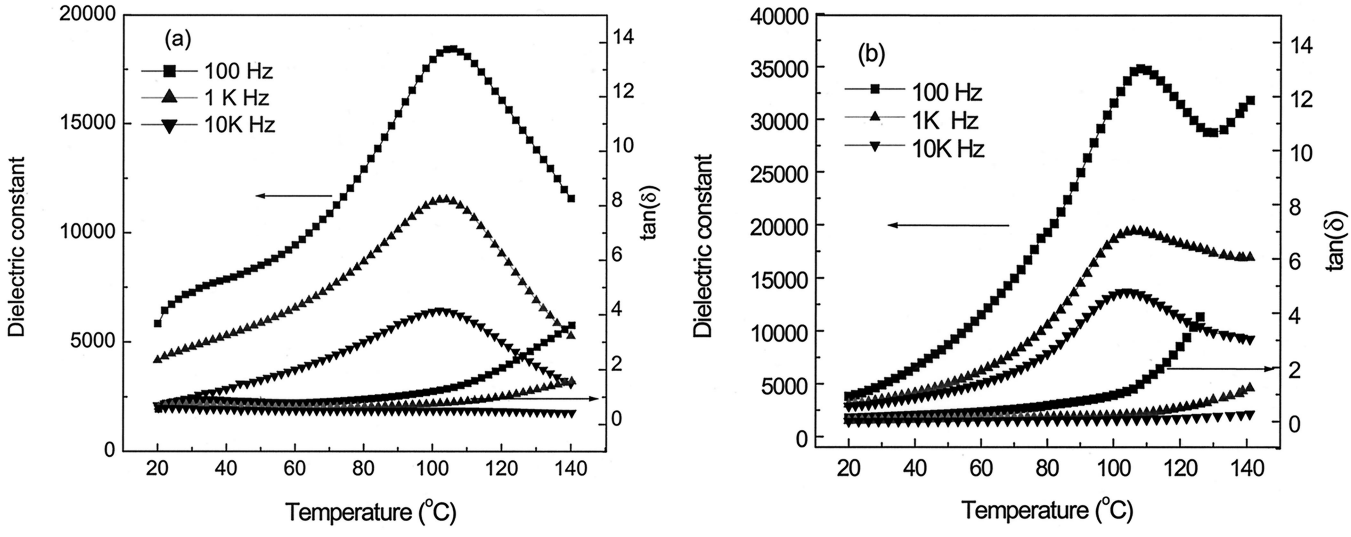

Fig. 12. Dielectric constant and dielectric loss as a function of test temperature for the PFN sintered at 1050°C and (a) derived from mechanical activation of mixed oxides of PbO, Fe_2O_3, and Nb_2O_5; and (b) derived from mechanical activation of the columbite precursor of PbO and $FeNbO_4$.

evolution with increasing temperature, as is shown in Figs. 9(a)–(d) and 10(a)–(d). On the other hand, the bulk resistance of the PFN derived from mixed oxides is much smaller than that of the PFN derived from columbite precursor. As a result of the high conductivity and Fe^{3+}/Fe^{2+} hopping, the former demonstrates an unrealistically high dielectric constant and extremely high dielectric loss.

The dielectric constant and dielectric loss, as a function of test temperature for the PFN sintered at 1050°C and derived from the mixed oxides and columbite precursor, are shown in Figs. 12(a) and (b), respectively. Both materials exhibit an apparent frequency dispersion in dielectric constant, confirming their relaxor behavior. A Curie temperature of 105°C was measured for the PFN derived from the mixed oxides, in contrast to 107°C for the PFN ceramic derived from the columbite precursor when both were measured at 100 Hz. The former exhibits a lower dielectric constant and a slightly higher dielectric loss than those of the latter, because of the higher conductivity in association with the compositional inhomogeneity, as described above.

IV. Conclusion

Mechanical activation has been successfully applied to the synthesis of nanocrystallite PFN from mixed individual oxides and a columbite precursor. A well-established nanocrystallite PFN phase of ~5–15 nm in size was obtained from both types of starting materials. However, the material derived from the mixed oxides is unstable during calcination at temperatures between 500° and 900°C, and partially decomposes into a pyrochlore phase. Therefore, it exhibits a lower sintered density at sintering temperatures ranging from ~950°–1150°C. In contrast, the nanocrystalline PFN phase derived from the columbite precursor is stable against the thermal treatment, and it remains a crystalline phase in the temperature range of 500°–900°C. Improved sintering behavior and different dielectric properties are observed in the PFN derived from the columbite precursor, in comparison to those of the PFN derived from mixed oxides of PbO, Fe_2O_3, and Nb_2O_5. The above differences between the PFN derived from the two types of starting materials can be accounted for by the composition inhomogeneity in the PFN derived from mixed oxides, as was confirmed by studies using Raman spectrometry.

References

[1]M. Nakano, K. Suzuki, T. Miura, and M. Kobayashi, "Low Temperature Fireable Dielectric Material $Pb(Fe_{2/3}W_{1/3})O_3$–$(Pb,Ca)(Fe_{1/2}Nb_{1/2})O_3$ for Microwave Use," *Jpn. J. Appl. Phys., Part B*, **32**, [9B] 4314–18 (1993).

[2]T. R. Shrout and A. Halliyal, "Preparation of Lead-Based Ferroelectric Relaxor for Capacitors," *Am. Ceram. Soc. Bull.*, **66** [4] 704–11 (1987).

[3]H. H. Lee and W. K. Choo, "A Phase Analysis in Pseudobinary $Pb(Fe_{1/2}/Nb_{1/2})O_3$–$Pb(Mg_{1/2}/W_{1/2})O_3$ Solid Solution," *J. Appl. Phys.*, **52** [9] 5767–73 (1981).

[4]V. A. Bokov, I. E. Myl'nikova, and G. A. Smolenskii, "Ferroelectric Anti-Ferromagnetics," *Phys., JETP*, **15**, 447–49 (1962).

[5]M. Jenhi, E. H. Elghadraoui, I. Bali, M. Elaatmani, and M. Rafiq, "Reaction Mechanism in the Formation of Perovskite $Pb(Fe_{1/2}Nb_{1/2})O_3$ by Calcining of Mixed Oxide (CMO)," *Eur. J. Solid State Inorg. Chem.*, **35**, 221–30 (1998).

[6]S. Ananta and N. W. Thomas, "A Modified Two-Stage Mixed Oxide Synthetic Route to Lead Magnesium and Niobate and Lead Iron Niobate," *J. Eur. Ceram. Soc.*, **19**, 155–63 (1999).

[7]P. Griesmar, G. Papin, C. Sanchez, and J. Livage, "Sol–Gel Synthesis of PFN Ceramics ($Pb(Fe_{1/2}Nb_{1/2})O_3$)," *J. Mater. Sci. Lett.*, **9**, 1288–99 (1990).

[8]C. C. Chiu, C. C. Li, and S. B. Desu, "Molten Salt Synthesis of a Complex Perovskite $Pb(Fe_{1/2}Nb_{1/2})O_3$," *J. Am. Ceram. Soc.*, **74** [1] 38–41 (1991).

[9]G. Guzman and M. A. Aegerter, "Synthesis of Ferroelectric Perovskite through Aqueous-Solution Techniques," *J. Mater. Sci.*, **28**, 5510–15 (1993).

[10]Y. Yoshikawa, "Chemical Preparation of Lead Containing Niobium Powders," *J. Am. Ceram. Soc.*, **79** [9] 2417–21 (1996).

[11]J. S. Benjamin, "Mechanical Alloying," *Sci. Am.*, **234**, 40–48 (1976).

[12]P. S. Gilman and J. S. Benjamin, "Mechanical Alloy," *Annu. Rev. Mater. Sci.*, **13**, 297–300 (1983).

[13]J. Ding, T. Tsuzuki, and P. G. McCormick, "Ultrafine Alumina Particles Prepared by Mechanochemical/Thermal Processing," *J. Am. Ceram. Soc.*, **79** [11] 2956–58 (1996).

[14]J. Wang, J. M. Xue, D. M. Wan, and W. B. Ng, "Mechanochemically Synthesized Lead Magnesium Niobate," *J. Am. Ceram. Soc.*, **82** [5] 1358–60 (1999).

[15]J. Wang, D. M. Wan, J. M. Xue, and W. B. Ng, "Synthesizing Nanocrystalline $Pb(Zn_{1/3}Nb_{2/3})O_3$ Powders from Mixed Oxides," *J. Am. Ceram. Soc.*, **82** [2] 477–79 (1999).

[16]S. K. Ang, J. Wang, D. M. Wan, J. M. Xue, and L. T. Li, "Mechanical Activation-Assisted Synthesis of $Pb(Fe_{2/3}W_{1/3})O_3$," *J. Am. Ceram. Soc.*, **83** [8] 1575–80 (2000).

[17]H. P. Klug and L. E. Alexander, *X-ray Diffraction Procedures for Polycrystalline and Amorphous Materials*; pp. 491–538. Wiley, New York, 1954.

[18]M. P. Kassarjian, R. E. Newnham, and J. V. Biggers, "Sequence of Reactions during Calcining of Lead-Iron Niobate Dielectric Ceramics," *Am. Ceram. Soc. Bull.*, **64** [8] 1108–11 (1985).

[19]J. Wang, J. M. Xue, D. M. Wan, and W. B. Ng, "Mechanicalchemical Fabrication of Single Phase PMN of Perovskite Structure," *Solid State Ionics*, **124**, 271–79 (1999).

[20]D. Wan, J. Xue, and J. Wang, "Mechanochemical Synthesis of $0.9[0.6Pb(Zn_{1/3}Nb_{2/3})O_3 \cdot 0.4Pb(Mg_{1/3}Nb_{2/3})O_3] \cdot 0.1PbTiO_3$," *J. Am. Ceram. Soc.*, **83** [1] 53–59 (2000).

[21]E. M. Levin, C. R. Robbins, and H. F. McMurdie, p. 83 (Fig. 148) in *Phase Diagrams for Ceramists*, Vol. 1. American Ceramic Society, Columbus, OH, 1964.

[22]D. L. A. de Faria, S. V. Silva, and M. T. de Oliveira, "Raman Microspectroscopy of Some Iron Oxides and Oxyhydroxides," *J. Raman Spectrosc.*, **28** [11] 873–78 (1997).

[23]J. Wang, J. M. Xue, and D. M. Wan, "How Different is Mechanical Activation from Thermal Activation? A Case Study with PZN and PZN-Based Relaxors," *Solid State Ionics*, **127** [1–2] 169–75 (2000).

[24]P. Bellon and R. S. Averback, "Nonequilibrium Roughening of Interface in Crystals under Shear: Application to Ball Milling," *Phys. Rev. Lett.*, **74** [10] 1819–22 (1995).

[25]M. Stanislaw, *Defect and Diffusion in Solids: An Introduction*; p. 392. Edited by C. Laird. Elsevier, Barking, Essex, U. K., 1980.

[26]S. E. Lee, J. M. Xue, D. M. Wan, and J. Wang, "Effect of Mechanical Activation on the Sintering and Dielectric Properties of Oxide-Derived PZT," *Acta Mater.*, **47** [9] 2633–39 (1999).

[27]S. Kim, G. S. Lee, T. R. Shrout, and S. J. Venkataramani, "Fabrication of Fine-Grain Piezoelectric Ceramics using Reactive Calcinations," *J. Mater. Sci.*, **26** [16] 4411–15 (1991).

[28]G. C. Kuczynski, *Sintering and Related Phenomena*; p. 685. Edited by G. C. Kuczynski, N. A. Hooton, and C. F. Gibbon. Gordon and Breach, New York, 1967.

[29]S. Ananta and N. W. Thomas, "Relationships between Sintering Conditions, Microstructure and Dielectric Properties of Lead Iron Niobate," *J. Eur. Ceram. Soc.*, **19**, 1873–81 (1999).

[30]A. K. Jonscher, *Dielectric Relaxation In Solids*; p. 247. Chelsea Dielectrics Press, London, U. K., 1983.

[31]X. R. Wang, Z. H. Gui, H. Li, and X. W. Zhang, "Mössbauer Study on Valence State of Iron Ions," *Mater. Lett.*, **20** [1–2] 75–78 (1994).

[32]D. Drazic, M. Trontelj, and D. Kolar, "Correlation between Microstructure and Electrical Conductivity and Electrical Conductivity in $Pb(Fe_{1/2}Nb_{1/2})O_3$–$Pb(Fe_{2/3}W_{1/3})O_3$–$Pb(Zn_{1/3}Nb_{2/3})O_3$ Relaxor Ferroelectrics," *Mater. Sci. Eng., B*, **26** [2–3] 189–96 (1994). □